Vortex states and magnetic anisotropy in single-crystal $La_{2-x}Sr_xCuO_4$ studied by torque magnetometry

S. Kohout,* T. Schneider, J. Roos, and H. Keller
Physik-Institut, Universität Zürich, Winterthurerstrasse 190, 8057 Zürich, Switzerland

T. Sasagawa and H. Takagi
Department of Advanced Materials Science, University of Tokyo, 5-1-5 Kashiwanoha, Kashiwa, Chiba 277-8561, Japan
(Received 15 April 2007; published 13 August 2007)

The cuprate superconductors have highly anisotropic, layered structures. This causes the flux lattice penetrating them in the intermediate state to undergo dramatic changes when the direction of the applied magnetic field approaches the CuO_2 planes. We present highly sensitive torque measurements on tiny $La_{2-x}Sr_xCuO_4$ single crystals showing these regimes of vortex structure and their influence on the determination of the magnetic anisotropy parameter γ. Systematic measurements of torque as a function of magnetic field magnitude and orientation at various temperatures below T_c made it possible to determine the conditions under which the structural changes occur, allowing a reliable determination of γ. The values of γ obtained for $La_{2-x}Sr_xCuO_4$ as a function of doping x, covering the whole doping regime (underdoped, optimally doped, and overdoped), are in good agreement with earlier results, indicating a flow toward quasi-two-dimensionality in the underdoped limit.

DOI: 10.1103/PhysRevB.76.064513 PACS number(s): 74.25.Qt, 74.25.Ha, 74.72.Dn, 75.30.Gw

I. INTRODUCTION

The mixed state in type-II superconductors, where magnetic flux enters a sample in form of single flux quantum vortices, is often used to extract and investigate various superconducting properties. Most of the models for these properties are based on a continuous anisotropic description. However, a lot of attention has always been attributed to the layered structure of these materials. A rich phase diagram has evolved from such calculations, and measurements have been found to confirm such effects. Lawrence and Doniach[1] were the first to account for the layered structure and proposed a description, similar to the Ginzburg-Landau theory, but specifically discretizing the equations along the c direction perpendicular to the CuO_2 planes. Others based their calculations upon this work and found indications for strong intrinsic pinning (lock-in) if the applied magnetic field is oriented close to the CuO_2 planes.[2–4] Observations of lock-in were made on various layered superconductors, including cuprates and organic superconductors.[5–10] Extending a proposition on the breakdown of the Abrikosov vortex lattice close to the CuO_2 planes in strongly anisotropic superconductors by Kes *et al.*,[11] Theodorakis[12] calculated in detail a model where four different vortex states are assumed depending on whether the applied field components parallel and perpendicular to the superconducting planes are above or below the respective lower critical fields $H_{c1}^{\parallel}$ and $H_{c1}^{\perp}$. Further calculations[4,11,12] lead to the prediction that the ordinary Abrikosov-type vortex lattice transforms first into a lattice of kinked Josephson vortices along the CuO_2 planes before finally locking in. A comprehensive summary of the theoretical work on this transition and lock-in is given by Blatter *et al.*[13]

In this paper, we present systematic measurements of the cuprate superconductor $La_{2-x}Sr_xCuO_4$ using highly sensitive torque magnetometry. Torque measurements are highly sensitive to the transverse magnetization perpendicular to an applied magnetic field and therefore well suited for investigations of anisotropic magnetic properties. Five single-crystal samples with different Sr contents, covering the underdoped, optimally doped, and overdoped regions, were investigated at temperatures below T_c and in fields up to 1.5 T. Due to increased irreversibility effects at low temperatures, only measurements within about 5 K below T_c were performed. Clearly visible systematics of the appearance of Josephson vortices and lock-in as a function of field strength, field orientation, and temperature is reported. Thanks to this systematics, we can clearly assign the peaks in angle-dependent torque measurements to the Josephson-type vortices—on the contrary to previous interpretations,[6–8] where these were attributed to the lock-in directly. We show that the effective lock-in only occurs in a much narrower angle region.

An important property of layered superconductors is the anisotropy parameter $\gamma=(m_c^*/m_{ab}^*)^{1/2}$, where m_c^* and m_{ab}^* are the effective supercarrier masses for currents flowing along the c axis and in the ab plane, respectively. It turns out that a precise determination of γ is problematic due to the appearance of the Josephson vortices. Here, we present a reliable procedure for the extraction of an accurate value of γ from magnetic torque measurements.

II. EXPERIMENTAL DETAILS

Single crystals of $La_{2-x}Sr_xCuO_4$ were grown using the traveling solvent floating zone technique.[14] Underdoped ($x=0.07, 0.125$), optimally doped ($x=0.15$), and overdoped ($x=0.19, 0.23$) single-crystal samples were prepared. Microcrystals of about $100\times100\times50$ μm^3 size were broken from these crystals. Due to their approximate cube shape, the demagnetizing factor $\nu\approx0.3$ for a sphere was used for calcu-

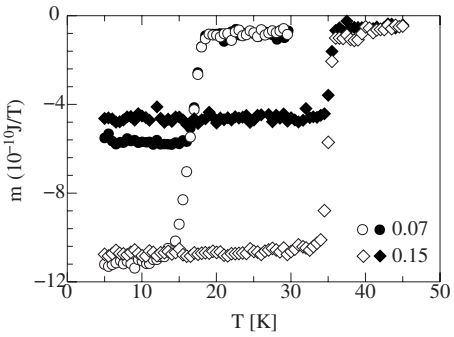

FIG. 1. Magnetization curves of two single-crystal $La_{2-x}Sr_xCuO_4$ samples ($x=0.07$ and $x=0.15$) obtained at $\mu_0 H = 1$ mT with the field parallel to the c axis. Closed and open symbols denote measurements obtained in field cooling and zero-field cooling modes, respectively.

lations where it appears. Low-field (1 mT) superconducting quantum interference device (SQUID) measurements in field cooling and zero-field cooling modes were performed to characterize the crystals. The transitions were sharp with transition widths (10%–90%) of $\Delta T \approx 0.2-1.0$ K and showed Meissner fractions between 20% and 50%, respectively. Typical low-field (1 mT) magnetization measurements of single-crystal $La_{2-x}Sr_xCuO_4$ ($x=0.07$ and $x=0.15$) are shown in Fig. 1.

A custom built torquemeter[15] was used to determine the sample's magnetic moment **m** from the torque

$$\boldsymbol{\tau} = \mu_0 \mathbf{m} \times \mathbf{H} \tag{1}$$

it experiences in an external magnetic field **H**. Torque magnetometry is well suited for investigations of anisotropic magnetic phenomena as found in high temperature superconductors.[5,8,16,17] It is complementary to most other magnetometry techniques in that it is only sensitive to $m_\perp$, the part of **m** perpendicular to the applied field, whereas most magnetometers measure the parallel component $m_\parallel$. A torque measurement is fast (one measurement takes only a fraction of a second) and reaches high sensitivities for $m_\perp$ in high fields due to the proportionality $\tau \propto H$. We used capacitive torque sensors[15] with a sensitivity of well below 10^{-12} N m. The system consists of a flow cryostat between the poles of a rotatable iron yoke magnet ($\mu_0 H_{\max} = 1.5$ T). It is fully computer controlled and allows efficient measurement taking.[18]

At a fixed temperature, magnetic torque measurements $\tau(H, \theta_{\text{fix}})$ were performed at various fixed field orientations θ_{fix} as a function of field magnitude H. Each field scan consisted of torque measurements during continuous increasing (τ_{inc}) and decreasing (τ_{dec}) field sweeps from 0 to 1.5 T. The average $\tau_{\text{rev}} = (\tau_{\text{inc}} + \tau_{\text{dec}})/2$ was then analyzed. Such field scans were performed at roughly 30 different field orientations on each crystal at about six different temperature settings. A complete background measurement well above T_c was taken for each crystal and subtracted from the data prior to analysis.

III. THEORETICAL BACKGROUND

The data were analyzed within the framework of the phase transition approach of Schneider and Singer,[19] where critical thermal fluctuations close to T_c are investigated, leading to universal relations. These critical properties allow the cuprates to be assigned to the three-dimensional (3D)-*XY* universality class.[19] The torque signal below T_c and for small fields then adopts the form[19]

$$\tau = m_0(1-\gamma^{-2})\frac{\sin(2\theta)}{\varepsilon_\gamma(\theta)}\mu_0 H \ln\left(\frac{H}{H_0}\varepsilon_\gamma(\theta)\right), \tag{2}$$

with

$$m_0 = \frac{-Q_3^- C_{3,0}^- k_B T V}{2\Phi_0 \xi_c^-}, \quad H_0 = \frac{\Phi_0}{\mu_0 (\xi_{ab}^-)^2}, \tag{3}$$

and

$$\varepsilon_\gamma(\theta) = \sqrt{\cos^2\theta + \gamma^{-2}\sin^2\theta}. \tag{4}$$

Generally, m_0, H_0, and γ are used as fitting parameters. Here, ξ_c^- and ξ_{ab}^- are the correlation lengths along and perpendicular to the c axis, respectively, and $\gamma = \xi_{ab}^-/\xi_c^-$ is the anisotropy parameter. The " $^-$" indicate that critical properties upon approaching T_c from below are investigated. V denotes the sample volume, H is the magnetic field magnitude, and θ is the angle it encloses with the sample's c axis. Φ_0 is the magnetic flux quantum and $Q_3^- C_{3,0}^- \approx 0.69$ is a universal constant for the 3D-*XY* universality class in the limit $T \to T_c$ and $H \to 0$.[20,21] In order for Eq. (2) to be applicable, the scaling variable

$$\mathcal{Z} = \frac{H}{H_0}\varepsilon_\gamma(\theta) \tag{5}$$

has to be small ($\mathcal{Z} \ll 1$), because for $\mathcal{Z} > 0.32$, magnetic field induced finite size effects[22] become important and cause a modification of the shape of $\tau(H, \theta)$. Equation (2) is found to agree well with measured data, except for angles $\theta \approx 90°$, where deviations are often observed [see Fig. 2(b)]. Since torque τ was measured at fixed angle θ as a function of magnetic field H, the form

$$\tau = m_\theta \mu_0 H \ln(H/H_\theta) \tag{6}$$

of Eq. (2) for a constant angle θ was used to fit the data. Regions of data where this model can be applied are easily identified by the linear dependence of τ_{rev}/H vs $\ln(H)$. The extracted parameters m_θ and H_θ are subsequently fitted to their respective angle dependence,

$$m_\theta = m_0(1-\gamma^{-2})\sin(2\theta)/\varepsilon_\gamma(\theta) \tag{7}$$

and

$$H_\theta = H_0/\varepsilon_\gamma(\theta), \tag{8}$$

in order to obtain m_0, H_0, and γ.

The specialties due to the layering are not encompassed in this general description. Calculations based on the vortex structure, however, have been used for a long time to describe torque data. Kogan's[23] description of the torque acting on a type-II superconductor for fields $H_{c1} \ll H \ll H_{c2}$ reads as

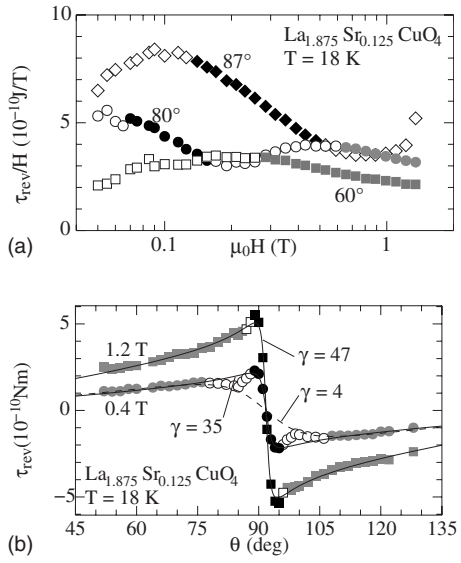

FIG. 2. Torque measurements $\tau_{\mathrm{rev}}(H,\theta_{\mathrm{fix}})$ of an underdoped $La_{2-x}Sr_xCuO_4$ ($x=0.125$) single-crystal sample at 18 K. (a) Part of the whole data set ($\theta=60°$, 80°, and 87°) plotted as τ_{rev}/H vs $\ln H$, revealing linear regions (filled black and gray symbols) according to Eq. (6). Data points belonging to high-field linear regions (ordinary, tilted vortex lattice) are filled gray. Those belonging to low-field linear regions (kinked vortices) are filled black. (b) Another part of the same data set plotted as τ_{rev} vs θ for $\mu_0 H=0.4$ T (circles) and $\mu_0 H=1.2$ T (squares). The meaning of the symbol filling is the same as in (a). Curves represent fits to Eq. (2). The strongly differing values obtained for γ illustrate the difficulty of its determination.

$$\tau = \frac{VH\Phi_0}{8\pi\lambda_{ab}^2} f_K(\vartheta), \tag{9}$$

with

$$f_K(\vartheta) = (1-\gamma^{-2})\frac{\sin\vartheta\cos\vartheta}{\varepsilon(\vartheta)}\ln\left(\frac{L\beta}{\xi_c\gamma\sqrt{\varepsilon(\vartheta)}}\right). \tag{10}$$

The angle ϑ is measured between the applied field and the CuO_2 planes, $L=\sqrt{(\Phi_0/B)}$ is the intervortex distance, and β is a constant of order unity. These results were obtained assuming a lattice of Abrikosov-type vortices. We note that the functional dependence of τ on H and θ of Eqs. (2) and (9) is the same. Theodorakis[12] investigated the case where the flux enters the sample in form of kinked vortices made of Josephson-type vortices between the CuO_2 layers interconnected by pancake vortices. His formula for the magnetic torque reads very similarly, replacing $f_K(\vartheta)$ by

$$f_T(\vartheta) = (1-\gamma^{-2})\frac{\sin\vartheta\cos\vartheta}{\varepsilon(\vartheta)}\ln\left(\frac{L\beta}{d\gamma\sqrt{\varepsilon(\vartheta)}}\right) + \mathrm{sgn}(\vartheta)\ln\left(\frac{d}{\xi_c}\right) \tag{11}$$

in Eq. (9) with d being the distance between the CuO_2 layers. The field dependence remains logarithmic with a different slope, though the angle dependence is modified by the additional term. At very small angles $\vartheta<\vartheta_L$ below the lock-in angle ϑ_L, the vortices lie fully between the CuO_2 layers, and the torque becomes independent of specific superconducting parameters and assumes a quadratic field dependence

$$\tau = \vartheta\frac{VH^2\mu_0}{2\nu}, \tag{12}$$

as calculated by Maslov and Pokrovsky.[24] The demagnetizing factor ν along the applied field direction makes comparison with experiments difficult, because it is difficult to estimate the effect of demagnetization for an arbitrarily shaped sample.

IV. RESULTS

Each field dependent measurement $\tau_{\mathrm{rev}}(H,\theta_{\mathrm{fix}})$ was investigated separately, regarding the applicability of Eq. (6), by plotting τ_{rev}/H vs $\ln H$, as shown in Fig. 2(a) for three different angles. Linear regions where Eq. (6) can be fitted are emphasized by gray and black filled symbols. At low angles ($\theta=60°$), only one such region was found [gray squares in Fig. 2(a)]. However, when θ approaches 90°, a second linear region appears at low fields (filled black circles, $\theta=80°$). This low-field region expands to higher fields very close to 90° (filled black diamonds, $\theta=87°$). Note that the high-field linear region of the $\theta=87°$ measurement lies above our maximum measurement field of $\mu_0 H=1.5$ T. However, measurements up to $\mu_0 H=7$ T in a SQUID magnetometer showed no change in slope $dm_{\parallel}/d(\ln H)$ of the magnetization parallel to the applied magnetic field. Therefore, we do not expect the perpendicular component $m_{\perp}$ measured by torque magnetometry to change either.

We emphasize that irreversibility $\tau_{\mathrm{inc}}-\tau_{\mathrm{dec}}$ is small in both linear regions. Different measurement conditions which affect the irreversibility did not change the results. Thus, we judge that irreversibility does not influence our results significantly. The points belonging to these high-field and low-field linear regions are easily associated with the smooth angular dependence at small angles and the steep increase close to $\theta=90°$ in Fig. 2(b), respectively. This steep increase has always been associated with lock-in, but our measurements suggest that it is due to the appearance of kinked vortices. The complete lock-in must therefore be restricted to a much smaller angular regime, identified by a quadratic field dependence. Such a quadratic field dependence can, in fact, be observed by plotting the slope $\frac{\Delta\tau}{\Delta\theta}$ ($\theta\approx 90°$) (effectively averaging over a few measured points at different angles) vs field H, as shown in Fig. 3.

The extents of the different regions observed in our measurements were determined for all measured angles, temperatures, and samples, leading to detailed maps in the θ-H planes. Such results are shown in Fig. 4 for an underdoped sample ($x=0.07$) at 13 K. The observed angle dependences of both the upper limit H_{l+} of the low-field linear region and the lower limit H_{h-} of the high-field linear region are well described by the relation

$$H = \frac{H_L}{|\cos\theta|}, \tag{13}$$

with a generic limiting field H_L as shown by the curves in Fig. 4. We note that Bulaevskii *et al.*[4] propose this equation

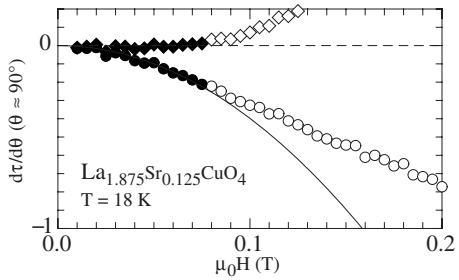

FIG. 3. The slope $\frac{\Delta\tau}{\Delta\theta}$ close to $\theta=90°$ as determined from measurements on a $La_{2-x}Sr_xCuO_4$ single crystal with $x=0.125$ as a function of magnetic field H and fitted with a quadratic function. Plotting the difference (diamonds) of data (circles) and fitted values (curve) clearly shows the region of quadratic dependence (filled symbols).

to describe the upper limit of lock-in with $H_L=H_{c1}^c(1-\nu_z)$, with ν_z being the sample's demagnetization factor perpendicular to the CuO_2 planes, and a crossover from the tilted vortex lattice to a combination of independent vortices perpendicular and parallel to the CuO_2 planes with $H_L=H_J(1-\nu_z)$. Unfortunately, our data quality is not sufficient to investigate the applicability of Eq. (13) to the lock-in regime. However, by fitting this function to the $H_{l+}(\theta)$ and $H_{h-}(\theta)$ data, $H_{L,l+}$ and $H_{L,h-}$ could be obtained for each measured sample and temperature, as shown in Fig. 5 (open and filled symbols, respectively). As is clearly visible in Fig. 5, $H_{L,l+}$ and $H_{L,h-}$ adhere to a linear temperature dependence. The slope $\alpha=\mu_0 dH_L/dT$ of this linearity allows us to compare the tilted-to-kinked vortex lattice transition field of the five differently doped samples. Values of α_{h-} are listed in Table I and clearly increase with increasing doping, which means that a stronger magnetic field is needed to drive the vortices from kinked to tilted in overdoped samples. The same tendency is shown by α_{l+}, but these values are not shown for brevity.

The linear regions found in $\tau_{\rm rev}(H,\theta_{\rm fix})/H$ vs $\ln H$ for different angles were independently fitted to Eq. (6). The resulting fitted parameters H_θ and m_θ of one data set of an

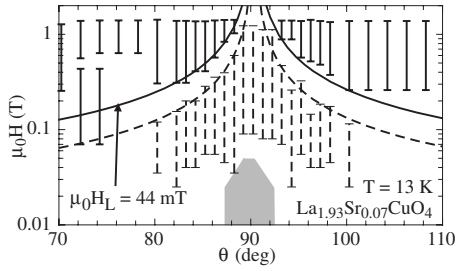

FIG. 4. Graphical representation of the field regions as displayed in Figs. 2(a) and 3 for an underdoped $La_{2-x}Sr_xCuO_4$ ($x=0.07$) single crystal. The vertical bars illustrate the lower and upper field limits of the linear regions. Dashed bars belong to the kinked phase, whereas solid bars represent the free tilted vortex lattice. The solid and dashed curves are fits of Eq. (13). The two solid bars at 72° and 74° probably belong to the same linear region, because they have very similar slopes $d(\tau_{\rm rev}/H)/d(\ln H)$. The gray region around 90° illustrates the occurrence of lock-in.

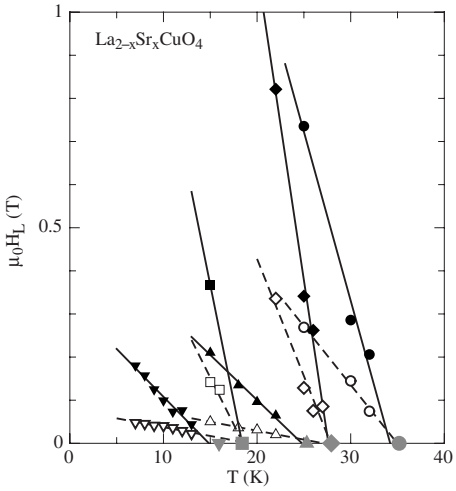

FIG. 5. Lower bound of the high-field linear region $H_{L,h-}$ (filled symbols) and upper bound of the low-field linear region $H_{L,l+}$ (open symbols), as obtained for single-crystal $La_{2-x}Sr_xCuO_4$ with various Sr contents x (∇, $x=0.07$; $\triangle$, $x=0.125$; $\bigcirc$, $x=0.15$; $\diamond$, $x=0.19$; $\square$, $x=0.23$). The large symbols on the abscissa represent the T_c's obtained as described in the text. Lines are linear fits with slopes $\alpha=\mu_0 dH_L/dT$.

underdoped sample ($x=0.07$) at fixed temperature ($T=13$ K) are shown in Fig. 6 as a function of angle. In principle, the anisotropy γ may be obtained from fits of Eqs. (7) and (8) to $m_\theta(\theta)$ and $H_\theta(\theta)$, respectively. However, there are difficulties: First of all, close to $\theta=90°$, points are missing for the tilted vortex lattice which are crucial for a reliable determination of γ due to its strong dependence on $\varepsilon_\gamma(\theta)$ [Eq. (4)] in this angle region. Second, the discrepancy between the γ values obtained from $m_\theta(\theta)$ and $H_\theta(\theta)$, respectively, is very large. It is particularly large for the kinked lattice, for which γ obtained from $H_\theta(\theta)$ diverges. The applicability of Eq. (2) to the kinked phase is therefore questionable. Consequently, physical conclusions drawn from results

TABLE I. Summary of some quantities obtained for single-crystal $La_{2-x}Sr_xCuO_4$ samples with various Sr contents x. T_c was obtained from linear extrapolation of m_0 vs T to $m_0=0$ (see text). The quantity $\alpha_{h-}=\mu_0 dH_{L,h-}/dT$ was obtained from linear fits to $H_{L,h-}$ vs T displayed in Fig. 5, and $T_{\rm max}$ is the temperature where the linear fit intersects the abscissa. The slope α_{l+} depends on doping in an analogous way at smaller absolute values. The anisotropy parameter γ was determined with the procedure described in the text.

x	T_c (K)	α_{h-} (mT/K)	$T_{\rm max}$ (K)	γ
0.070	17.67(19)	−22.2(19)	14.9(5)	73.5(2.0)
0.108	23.83(20)			37.8(1.0)
0.125	25.31(14)	−20.9(17)	24.8(6)	35.0(1.0)
0.150	35.18(37)	−78(12)	34.2(9)	19.0(1.0)
0.190	27.93(6)	−144(17)	27.6(5)	10.2(1.0)
0.230	18.41(14)	−108[a]		10.6(1.0)

[a]Slope obtained from one point and T_c only.

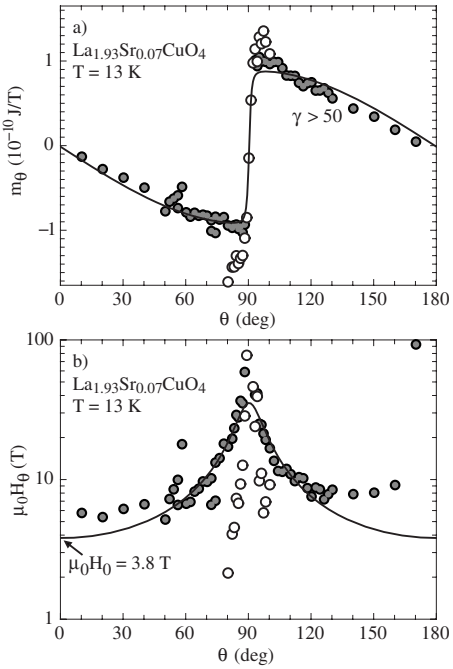

FIG. 6. The fitting parameters m_θ (a) and H_θ (b) as determined for a $La_{1.93}Sr_{0.07}CuO_4$ single crystal at 13 K as a function of the angle θ. Closed and open circles correspond to results from field regions of the tilted and the kinked vortex lattice, respectively. Curves in (a) and (b) are fits of Eqs. (7) and (8), respectively, to the tilted vortex lattice data.

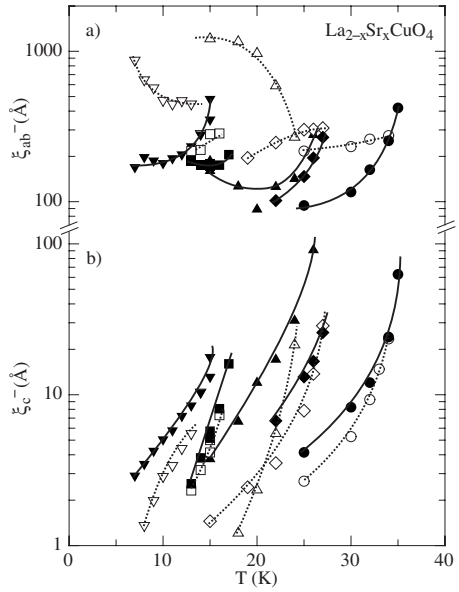

FIG. 7. (a) In-plane (ξ_{ab}^-) and (b) out-of-plane (ξ_c^-) correlation lengths as determined from m_0 and H_0 using Eq. (3) for single crystals of $La_{2-x}Sr_xCuO_4$ for various dopings x (∇, $x=0.07$; $\triangle$, $x=0.125$; $\bigcirc$, $x=0.15$; $\diamond$, $x=0.19$; $\square$, $x=0.23$). Filled and open symbols are obtained from measurements of the tilted and the kinked vortex lattice, respectively. Qualitatively, the difference between the correlation lengths for the two vortex lattice configurations (filled and open symbols) is larger for underdoped (triangles) than for overdoped (quadrilaterals) samples. Curves are guides to the eyes.

obtained in the kinked lattice must be treated with care. On the other hand, m_0 and H_0 obtained from fits of Eqs. (7) and (8) to $m_\theta(\theta)$ and $H_\theta(\theta)$, respectively, of the free, tilted vortex lattice (Fig. 6, filled circles) are largely independent of γ. This was checked by varying and holding γ while fitting the other parameters. Thus, for each sample and temperature, the parameters m_0 and H_0 can be obtained. From these, the in-plane and out-of-plane correlation lengths ξ_{ab}^- and ξ_c^- are determined by Eqs. (3), as shown in Fig. 7. As expected, the divergence of the correlation lengths upon approaching T_c is observed for the results obtained from the free, tilted vortex lattice. The difference between open and filled symbols in Fig. 7 shows that the qualitative difference between the tilted and the kinked vortex lattice is more pronounced in underdoped samples. The temperature dependence of the scaling variable $\mathcal{Z}$ [Eq. (5)], which must satisfy $\mathcal{Z} \ll 1$ in order to justify the use of Eq. (2), is plotted in Fig. 8. The average $\mathcal{Z}_{avg}=H_{avg}\varepsilon_\gamma(\theta)/H_0$ is shown, where H_{avg} is the average of the field region from which H_0 was obtained by fitting Eq. (6). As is clearly seen, this requirement is fulfilled for all measurements, except for temperatures very close to T_c. The critical value $\mathcal{Z} \approx 0.3$, where magnetic field induced finite size effects are expected to set in,[22] is shown as well.

As stated in the Introduction, the occurrence of kinked vortices inhibits a reliable determination of the anisotropy parameter γ. It may also cause a spurious field dependence when angle-dependent measurements $\tau_{rev}(H_{fix},\theta)$, taken at different fields and fitted with Eq. (2), are compared. The temperature dependence of H_L clearly shows that kinked vortices appear up to temperatures close to T_c (see Fig. 5). Therefore, for a reliable determination of γ, only measurements close to T_c and in high fields should be considered. For this reason, we fitted Eq. (2) to the angle dependence $\tau_{rev}(H_{fix},\theta)$ at various fixed fields H_{fix}. The resulting field dependent $\gamma(H)$ was averaged over the high-field region, where it is field independent. At low fields, however, some field dependence of γ is always observed. The resulting anisotropies γ obtained for the single-crystal samples investigated here are shown in Fig. 9 and listed in Table I. The

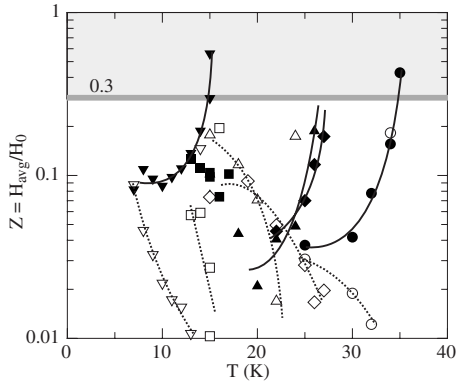

FIG. 8. Temperature dependence of the average scaling variable $\mathcal{Z}$ for single-crystal samples of $La_{2-x}Sr_xCuO_4$ for various Sr contents x. Symbols are the same as in Figs. 5 and 7. It is evident that Eq. (2) is valid over the whole temperature range, except for $T \lesssim T_c$ ($\mathcal{Z} \gtrsim 0.3$, gray region), where field induced finite size effects are expected to set in (Ref. 22).

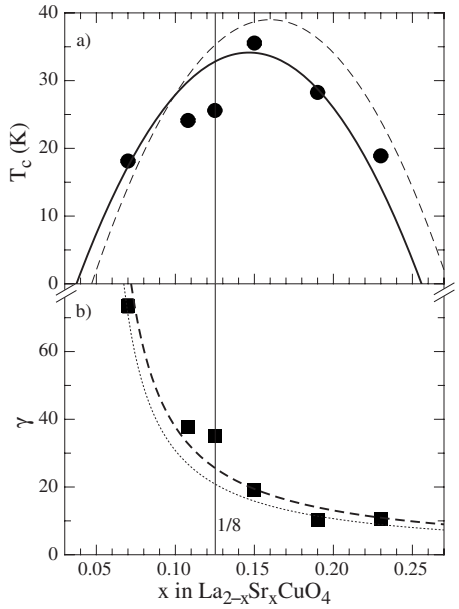

FIG. 9. (a) T_c and (b) anisotropy parameter γ of $La_{2-x}Sr_xCuO_4$ single crystals as a function of doping x, determined as described in the main text. (a) The solid parabola is a guide to the eyes. The dashed parabola serves as a comparison to the data shown in Fig. 1 of Ref. 30. (b) Both the dashed and the dotted curves are the ones shown in Fig. 1 of Ref. 30. The considerably lower T_c and higher γ of the two underdoped samples with nominal concentrations $x=0.108$ and $x=0.125$ could be interpreted by a lower effective doping of $x \approx 0.09$.

critical temperatures T_c shown in Figs. 5 and 9 and listed in Table I were obtained from linear extrapolations of $m_0(T)$, which is linear within error bars close to T_c. The doping dependence of T_c and γ follows approximately the empirical models proposed in Refs. 25–29. However, we observe a general shift of the T_c dome toward lower doping x and a generally lower T_c. The latter can be attributed to the fact that single crystals usually exhibit lower T_c's than powder samples. The lower T_c of the samples with nominal compositions $x=0.108$ and $x=0.125$ is in accordance with the dip of T_c observed close to $x=1/8$.[31] Our values of the anisotropy parameter γ for these samples lie above the general trend of the other samples (see Fig. 9). Both deviations may be interpreted such that the effective doping of these samples is considerably lower ($x \approx 0.09$). Plotted as T_c vs $1/\gamma$, all points fall on the universal parabola found for various cuprates.[30]

V. SUMMARY

The appearance of kinked vortices and the lock-in effect in the layered superconductor $La_{2-x}Sr_xCuO_4$ was studied extensively by means of torque magnetometry. Our measurements allowed us to identify the characteristic peaks of torque close to the CuO_2 planes with the appearance of kinked vortices—contrary to previous measurements which assigned them to the lock-in effect. In particular, the influence of these vortex configurations on the determination of the anisotropy parameter γ was investigated. Kinked vortices appear nearly up to the critical temperature T_c and can only be avoided in large magnetic fields. Thus, γ must be determined close to T_c in a field as large as possible. Values of the anisotropy parameter γ obtained this way show that it increases with decreasing doping x, indicating that the system becomes quasi-two-dimensional in the underdoped limit.[27,28] Even though the determination and interpretation of the correlation lengths $\xi^-_{ab,c}$ of the kinked phase are questionable, their difference to the $\xi^-_{ab,c}$ of the free vortex lattice can be regarded as a measure of how large the qualitative difference between the two phases is. As expected, we observe that the qualitative difference between the two phases becomes more pronounced toward the two-dimensional (2D) limit in the underdoped regime. However, the magnetic field needed to drive the kinked lattice to its free, tilted orientation decreases toward this 2D limit, implying that the tendency to form kinked vortices is weakened as the system becomes quasi-two-dimensional. The agreement with other measurements of the anisotropy γ shows that the procedure presented in this paper is well suited for the determination of γ from magnetic properties.

ACKNOWLEDGMENT

This work was partly supported by the Swiss National Science Foundation.

*kohout@physik.unizh.ch

[1] W. E. Lawrence and S. Doniach, in *Proceedings of the 12th International Conference on Low Temperature Physics, Kyoto, 1970*, edited by E. Kanda (Academic, New York, 1971), p. 361.
[2] M. Tachiki and S. Takahashi, Solid State Commun. **70**, 291 (1989).
[3] D. Feinberg and C. Villard, Phys. Rev. Lett. **65**, 919 (1990).
[4] L. N. Bulaevskii, M. Ledvij, and V. G. Kogan, Phys. Rev. B **46**, 366 (1992).
[5] D. E. Farrell, J. P. Rice, D. M. Ginsberg, and J. Z. Liu, Phys. Rev. Lett. **64**, 1573 (1990).
[6] S. Kawamata, N. Itoh, K. Okuda, T. Mochiku, and K. Kadowaki, Physica C **195**, 103 (1992).
[7] F. Steinmeyer, R. Kleiner, P. Müller, and K. Winzer, Physica B **194**, 2401 (1994).
[8] D. Zech, C. Rossel, L. Lesne, H. Keller, S. L. Lee, and J. Karpinski, Phys. Rev. B **54**, 12535 (1996).
[9] M. A. Avila, L. Civale, A. V. Silhanek, R. A. Ribeiro, O. F. de Lima, and H. Lanza, Phys. Rev. B **64**, 144502 (2001).
[10] K. Takahashi, T. Atsumi, N. Yamamoto, M. Xu, H. Kitazawa, and T. Ishida, Phys. Rev. B **66**, 012501 (2002).
[11] P. H. Kes, J. Aarts, V. M. Vinokur, and C. J. van der Beek, Phys. Rev. Lett. **64**, 1063 (1990).
[12] S. Theodorakis, Phys. Rev. B **42**, 10172 (1990).

[13] G. Blatter, M. V. Feigel'man, V. B. Geshkenbein, A. I. Larkin, and V. M. Vinokur, Rev. Mod. Phys. **66**, 1125 (1994).
[14] T. Sasagawa, K. Kishio, Y. Togawa, J. Shimoyama, and K. Kitazawa, Phys. Rev. Lett. **80**, 4297 (1998).
[15] C. Rossel, M. Willemin, A. Gasser, H. Bothuizen, G. I. Meijer, and H. Keller, Rev. Sci. Instrum. **69**, 3199 (1998).
[16] J. C. Martinez, S. H. Brongersma, A. Koshelev, B. Ivlev, P. H. Kes, R. P. Griessen, D. G. de Groot, Z. Tarnavski, and A. A. Menovsky, Phys. Rev. Lett. **69**, 2276 (1992).
[17] M. Willemin, C. Rossel, J. Hofer, H. Keller, Z. F. Ren, and J. H. Wang, Phys. Rev. B **57**, 6137 (1998).
[18] S. Kohout, J. Roos, and H. Keller, Meas. Sci. Technol. **16**, 2240 (2005).
[19] T. Schneider and J. M. Singer, *Phase Transition Approach to High Temperature Superconductivity* (Imperial College Press, London, 2000).
[20] J. Hofer, T. Schneider, J. M. Singer, M. Willemin, H. Keller, C. Rossel, and J. Karpinski, Phys. Rev. B **60**, 1332 (1999).
[21] J. Hofer, T. Schneider, J. M. Singer, M. Willemin, H. Keller, T. Sasagawa, K. Kishio, K. Conder, and J. Karpinski, Phys. Rev. B **62**, 631 (2000).
[22] T. Schneider, J. Supercond. **17**, 41 (2004).
[23] V. G. Kogan, Phys. Rev. B **38**, 7049 (1988).
[24] S. S. Maslov and V. L. Pokrovsky, Europhys. Lett. **14**, 591 (1991).
[25] M. R. Presland, J. L. Tallon, R. G. Buckley, R. S. Liu, and N. E. Flower, Physica C **176**, 95 (1991).
[26] J. L. Tallon, C. Bernhard, H. Shaked, R. L. Hitterman, and J. D. Jorgensen, Phys. Rev. B **51**, R12911 (1995).
[27] T. Schneider and H. Keller, Phys. Rev. Lett. **86**, 4899 (2001).
[28] T. Schneider, Physica B **326**, 289 (2003).
[29] T. Schneider, in *The Physics of Superconductors*, edited by K. Bennemann and J. B. Ketterson (Springer, Berlin, 2004), p. 111.
[30] T. Schneider, Phys. Status Solidi B **242**, 58 (2005), and references therein.
[31] P. G. Radaelli, D. G. Hinks, A. W. Mitchell, B. A. Hunter, J. L. Wagner, B. Dabrowski, K. G. Vandervoort, H. K. Viswanathan, and J. D. Jorgensen, Phys. Rev. B **49**, 4163 (1994).